American Mineralogist, Volume 81, pages 19–25, 1996

Dispersion relations of acoustic phonons in pyrope garnet: Relationship between vibrational properties and elastic constants

G. Artioli,[1] A. Pavese,[1] and O. Moze[2]

[1] Dipartimento di Scienze della Terra, Università di Milano, I-20133 Milan, Italy
[2] Dipartimento di Fisica, Università di Parma, I-43100 Parma, Italy

Abstract

Coherent inelastic neutron scattering measurements have been performed on a natural garnet pyrope from the Dora Maira Massif, Italian Western Alps, [$(Mg_{0.92}Fe_{0.05}Ca_{0.03})_3Al_2Si_3O_{12}$, space group $Ia\bar{3}d$, $Z = 8$, $a = 11.459$ Å] to determine the acoustic phonon-dispersion relations at room temperature. Phonon measurements have not previously been made on natural garnets, although the dispersion curves form a basis for developing and testing physically correct interatomic potentials for use in lattice dynamical models. Acoustic phonons propagating in the high-symmetry [100] and [110] directions were observed using the PRISMA spectrometer installed at the ISIS Neutron Spallation Source, U.K. The inelastic scans were performed around the (660), (080), (860), (10,6,0), and (0,10,0) Bragg points: Two transverse acoustic and one longitudinal acoustic phonon branches were measured. The observed acoustic phonon frequencies are in good agreement with those calculated on the basis of a semiempirical interatomic potential model. As a check, the elastic constants obtained from the slopes of the acoustic phonon branches are comparable with previous measurements obtained by Brillouin spectroscopy, although their large estimated errors reflect the complexity of the experimental measurements of phonon-dispersion curves on pyrope garnets.

Introduction

The vibrational properties of many minerals of great geophysical interest have been widely studied by optical spectroscopy (IR and Raman) techniques, therefore limiting the analyses to modes that are active only at the Brillouin zone center. Neutron inelastic scattering data, which provide information throughout the Brillouin zone, are remarkably scarce even for the basic rock-forming silicates. Data have been published only for quartz (Elcombe 1967; Boysen 1980; Strauch and Dorner 1993), forsterite (Ghose et al. 1987; Rao et al. 1988), fayalite (Ghose et al. 1991; Price et al. 1991), calcite (Cowley and Pant 1973; Dove et al. 1992; Hagen et al. 1992), sapphire (Bialas and Stolz 1975; Schober et al. 1993), enstatite (Boysen et al. 1991), muscovite (Collins et al. 1993), andalusite (Winkler and Buehrer 1990), leucite (Boysen 1990), and analcime (Line et al. 1994). By measuring frequencies throughout the Brillouin zone a greater understanding of their physical properties becomes possible.

The lattice vibrations within the frequency region accessed by coherent inelastic neutron scattering constitute a vital link, through lattice dynamics and statistical mechanics, between interactions at the atomic level and macroscopic thermodynamic quantities (Salje and Werneke 1982; Parker and Price 1988; Ghose et al. 1992; Pavese et al. 1992; Catti et al. 1993). Such data are important for the refinement of reliable interatomic potentials, which are increasingly utilized in the investigation of mineral properties and in the understanding of mineral behavior. They allow investigations at temperature and pressure conditions that are not experimentally accessible, following thermo-baric equilibration through structural relaxation (Wall et al. 1993; Catti et al. 1993; Pavese et al. in preparation), as well as detailed lattice dynamical studies of minerals (Winkler et al. 1991; Pilati et al. 1993a, 1993b).

Measurements of the phonon frequencies away from the Brillouin zone center are important because they complement the data obtained at the zone center by optical spectroscopy. Inelastic neutron scattering allows observation of modes that are not IR and Raman active. Although garnet is a major rock-forming mineral of importance for crustal and upper-mantle geophysical and petrological processes, no data, except for those for the zone center, are available in the literature. Indeed, taking into account that there are $3N$ active modes (where N is the number of atoms in the primitive unit cell), and that no selection rules exist for inelastic neutron spectroscopy, the measurement of phonon-dispersion curves on garnet is a demanding task because garnet ($X_3Y_2Si_3O_{12}$, $Z = 8$, space group $Ia\bar{3}d$) has 80 atoms in the primitive cell, and therefore 240 active modes must be resolved for each reciprocal space point.

We selected the end-member garnet pyrope ($a = 11.459$ Å at 293 K) for the present study because (1) it is avail-

0003–004X/96/0102–0019$05.00

able in large, natural single crystals (Chopin 1984; Schertl et al. 1991), (2) it has recently been studied by X-ray and neutron diffraction over an extended temperature range for the accurate evaluation of the atomic displacement parameters (Armbruster et al. 1992; Pavese et al. 1995), and (3) it has been the subject of structure modeling by lattice dynamical calculations (Winkler et al. 1991; Gramaccioli et al. personal communication).

In the present work we report the results of coherent inelastic neutron scattering measurements of the phonon-dispersion relations on a large, natural pyrope single crystal from the Dora Maira massif. The data are compared with lattice dynamical calculations using interatomic potentials available in the literature (Winkler et al. 1991), and the slopes of the dispersion curves are analyzed to extract information on the elastic properties of the mineral. The potentials employed in these simulations have been used extensively in the literature to model the physical properties of garnets, and the present testing of these interatomic potentials against observed phonon-dispersion curves is important, particularly for the modeling of physical properties at low-T conditions where acoustic phonon modes represent the major contribution to the thermodynamic properties. For example, the accurate prediction of physical behavior at low temperatures is crucial for clarifying the relationship between dynamical anomalies of the $^{[8]}$Mg cations and thermodynamic quantities such as specific heat and entropy (Haselton and Westrum 1980; Hofmeister and Chopelas 1991).

Experimental procedure

Presently available neutron sources are rather weak in terms of total neutron flux at the sample, and the inelastically scattered signal is a modest fraction of the total neutron cross section of the sample. Furthermore, in complex structures such as garnets, the total scattering intensity is subdivided among many modes, and so the signal of each one is very weak and its detection is experimentally demanding. Therefore, large single crystals (on the order of several cubic centimeters in volume) are desirable for inelastic neutron measurements at research reactors or pulsed neutron sources. Pyrope crystals of this size cannot be synthesized, thus we utilized a large, natural single crystal of the Dora Maira pyrope (approximately 20 cm^3 in volume), which is the only reported natural garnet with a very small amount (approximately 8%) of almandine-grossular components.

The measurements were performed on the PRISMA spectrometer installed at the Intense Spallation Isotope Source (ISIS) at the Rutherford Appleton Laboratory, Chilton, U.K. Although the instrumental resolution is not ideally suited for the present experiment, a major advantage of this spectrometer is that it is possible to obtain an overview of the phonon-response function in the energy range from -20 to $+100$ meV (Andreani et al. 1987; Steigenberger et al. 1991; Sacchetti et al. 1994). This is important in the case of pyrope garnet because the complex structure of the mineral implies the presence of many phonon modes, the locations of which in $\mathbf{Q}$-ω space are not known a priori. In the actual experiment the energy region utilized to extract acoustic modes is ± 20 meV. The energy region above 20 meV was also analyzed, but the number of modes and the presence of multiphonon effects are such that detection of one-phonon signals is precluded given the present resolution of the instrument.

The inelastic-scattering scans were performed using 12 independent pyrolitic graphite analyzers equipped with ^{3}He detectors. The pyrope single crystal was oriented with a [001] axis vertical. Inelastic scans were performed at 293 K along the following high-symmetry directions: the [100] direction ([$\bar{1}$11], according to the primitive cell) around the (660), (860), and (10,6,0) Bragg points and the [110] direction ([001] in the primitive cell) around the (080) and (0,10,0) Bragg points. Typical measuring times were 15–18 h per scan; the long scan times were required because of the large $\mathbf{Q}$-ω area measured and the poor signal-to-noise ratio. The high background is partly caused by the presence of accessory minerals present in the pyrope crystal as impurity phases. Some of these contain H (e.g., muscovite, chloritoid, paragonite) and therefore considerably increased the total incoherent scattering cross section. The high background is also attributed to multiphonon effects. Figures 1a and 1b show two experimental scans, collected on two detectors in the energy range from -12 to -6 meV and from 2.5 to 9.5 meV, respectively, and reveal inelastic signals.

Several acoustic phonon modes were observed in the detector scans in the ± 20 meV energy transfer region. A Gaussian function was fitted to the phonon peaks in the energy scans. Although the correct instrumental function for PRISMA is a Kropf function (a Gaussian convoluted with an exponential function), we used a single Gaussian fit because the difference between these two functions, primarily evident around the trailing edge of the peak, is actually not significant for the present experimental data. Extracted energy-transfer values are plotted along the parabolic path of the corresponding detector in wavevector-energy ($\mathbf{Q}$-ω) space. These plots allow one to follow the phonon-dispersion curves in $\mathbf{Q}$-ω space, where $\mathbf{Q}$ is the change of the wavevector on scattering and ω is related to energy transfer by $\Delta E = \hbar\omega$. Figures 2a and 2b show two plots corresponding to scans along the [100] direction, around the (660) and (860) Bragg points, respectively.

A total of 54 single acoustic phonon modes were observed, corresponding to the three dispersion curves shown in Figures 3a–3c, which were readily interpreted by comparison with the calculated data. Additional peaks were observed but were assigned (on the basis of the calculated dispersion curves) to spurious energy-transfer processes (spurions), such as the incoherent scattering of the analyzer crystal triggered by an elastic Bragg peak of the sample (Hagen 1994), and not to single phonon modes.

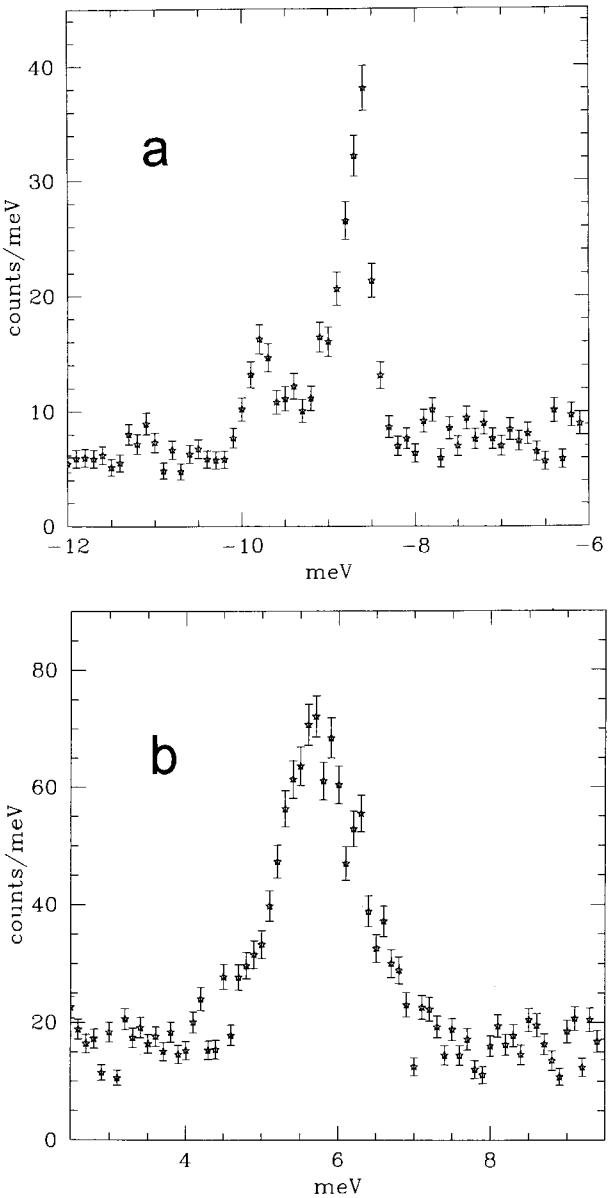

FIGURE 1. Inelastic signals collected on two detectors in energy-loss (**a**) and energy-gain (**b**) mode.

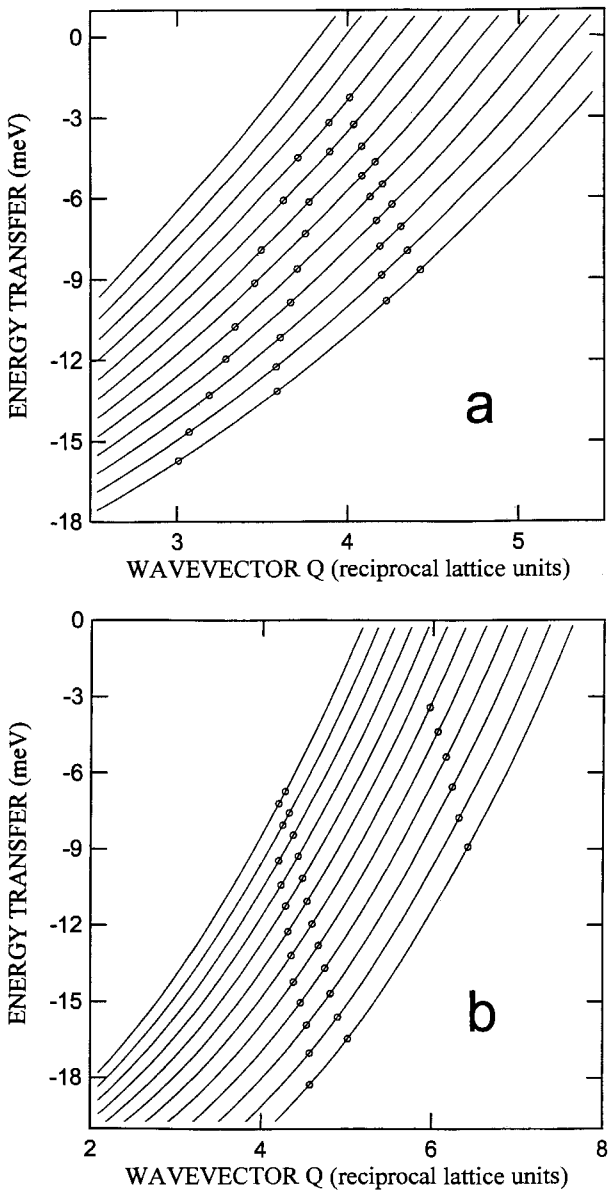

FIGURE 2. Phonon-dispersion curves for TA and LA phonons in pyrope in the [100] direction, with respect to the body-centered cell, around the Bragg points (660) (**a**) and (860) (**b**), respectively. The solid lines are the **Q**-ω trajectories traversed by the respective detectors.

SIMULATION TECHNIQUES

Numerical simulations play a fundamental role in the analysis of data from inelastic neutron scattering experiments because they allow one to distinguish and assign phonon modes. Because of the low signal-to-noise ratio owing to the presence of H, the presence of multiphonon effects, and the many frequencies, a reliable simulation of the vibrational modes and the corresponding scattering cross sections is essential for correct assessment and interpretation of the measurements. Simulation is also necessary to recognize, distinguish, and classify inelastic signals and to rule out those caused by impurities or spurions.

The theories of semiempirical potentials and lattice dynamics are employed to simulate the interatomic interactions, to compute the vibrational frequencies with the corresponding eigenvectors, and to evaluate the cross sections of inelastic processes. The interatomic interactions are modeled using a potential employed by Winkler et al. (1991) to study the lattice energy and lattice dynamics of some important aluminosilicate minerals, including pyrope. Because of the excellent level of transferability and

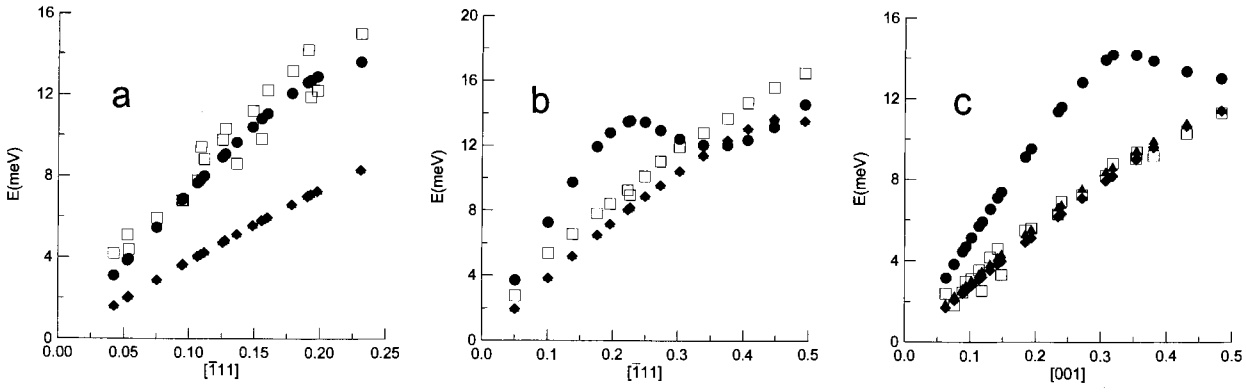

FIGURE 3. Experimental data (open squares) are plotted together with calculated acoustic phonon branches (solid symbols; triangles and diamonds are transverse modes, circles are longitudinal modes). (**a**) LA along [$\bar{1}$11], (**b**) TA along [$\bar{1}$11], and (**c**) TA along [001].

the good results reported by Winkler et al. (1991), the same potential was utilized in the present study without any optimization of its parameters. A brief description follows below.

All chemical species interact through the classical Coulomb electrostatic potential, using formal charges as suggested by Catlow (1988). The O charge is split into core and shell contributions, which interact reciprocally through a harmonic potential. A Born-like potential is assumed to account for repulsive energy for Al-O and O-O interactions, and, for the latter, a further dispersive term is added. The covalent contribution, present in the bonds involving $^{[6]}$Al or $^{[4]}$Si and the neighboring O atoms, is modeled by a further bond-bending term. The effect of bond-bending interactions is quite modest in the present calculation, and the bond-bending contribution from Al is therefore neglected. The values of the parameters of the described potential functions are derived from published works: Si-O and O-O bonds from Sanders et al. (1984), Al-O from Catlow et al. (1982), and Mg-O from Parker and Price (1988).

Using these potentials, the vibrational frequencies are calculated by classical lattice dynamics techniques (Dove 1993; Böttger 1983; Born and Huang 1954), together with the corresponding eigenvectors for selected **Q** points of reciprocal space. Such information allows estimation of the neutron coherent-scattering cross section for an inelastic process, characterized by a change **Q** in the wavevector ($\mathbf{Q} = \mathbf{K}_i - \mathbf{K}_f$, where $\mathbf{K}_i$ and $\mathbf{K}_f$ are the incident and final neutron wavevectors), by means of a straightforward integration over the energy and direction of the scattered neutrons, of the following equation (Lovesey 1984):

$$\frac{d^2\sigma}{d\Omega dE} \propto \frac{|\mathbf{K}_f|}{|\mathbf{K}_i|} \sum_{\mathbf{G}} \sum_{j,\mathbf{q}} \delta(\mathbf{Q} + \mathbf{q} - \mathbf{G}) \cdot \left| \sum_d b_d \exp[-W_d(\mathbf{Q}) + i\mathbf{Q}\cdot\mathbf{d}]\mathbf{K}\cdot\mathbf{e}_d^j(\mathbf{q}) M_d^{-1/2} \right|^2 \cdot \Big(n[\omega_j(\mathbf{q})]\delta[\omega + \omega_j(\mathbf{q})] + \{1 + n[\omega_j(\mathbf{q})]\}\delta[\omega - \omega_j(\mathbf{q})] \Big) / \omega_j(\mathbf{q}) \quad (1)$$

where δ is the Dirac function relating the **Q**, **q**, and **G** vectors; **G** is a reciprocal lattice vector; the **q** vector lies within the first Brillouin zone; d identifies each atom; W is the atomic Debye-Waller term; $\mathbf{e}^j(\mathbf{q})$ is the eigenvector of the frequency $\omega_j(\mathbf{q})$ evaluated at the point **q**; and b_d and M_d are the coherent-scattering cross section ($b_{Mg} = 0.5375$, $b_{Al} = 0.3449$, $b_O = 0.5805$, $b_{Si} = 0.4149 \times 10^{-12}$ cm; from Lovesey 1984) and the mass of atom d, respectively. By using the lattice dynamics formalism the Debye-Waller factor may be expressed as (Lovesey 1984)

$$W(\mathbf{K})_d = \hbar/(4NM_d) \cdot \sum_{j,\mathbf{q}} \frac{|\mathbf{K}\cdot\mathbf{e}_d^j(\mathbf{q})|^2\{2n[\omega_j(\mathbf{q})] + 1\}}{\omega_j(\mathbf{q})} \quad (2)$$

where symbols have the same meaning as above, $n[\omega_j(\mathbf{q})]$ is the Bose-Einstein distribution for the frequency j computed at each **q** point of reciprocal space, and N is the number of primitive cells present in the crystal.

A total of 27 weighted points were sampled throughout the reciprocal primitive cell to calculate the Debye-Waller factor for each atom in the pyrope structure and to evaluate the inelastic scattering cross section, by means of Equation 1. The computer program PARAPOCS (Parker and Price 1988) was modified to perform the calculations needed to study inelastic processes. Bearing in mind that $\omega(\mathbf{q}) = \omega(\mathbf{q} + \mathbf{G}) = \omega(-\mathbf{q})$ if **G** belongs to the reciprocal lattice, all our considerations may unambiguously refer to the experimental **Q** momentum transfer or to the **q** vector of the phonon mode.

DISCUSSION

All the well-characterized phonons were unambiguously interpreted as acoustic phonons because the active optic modes have higher energy transfer values near the

zone center. Transverse and longitudinal acoustic modes were classified through a careful analysis of the eigenvectors of the calculated phonons. The well-recognized phonons were then gathered in three sets and compared with the calculated acoustic branches in energy vs. **q** plots, where the **q** vectors are indexed according to the reciprocal primitive cell and χ indicates the position along the reciprocal vector. The plots are shown in Figures 3a–3c. Table 1 reports the observed and computed frequencies for each experimental **Q**-ω point.

In Figure 3a the experimental branch measured along the reciprocal space direction $\chi[\bar{1}11]$ is assigned to the only theoretical longitudinal acoustic mode existing in this direction; the other two acoustic transverse modes are degenerate and clearly do not match the observed data. The experimental data are poorly resolved in **Q**-ω space, particularly at energies higher than 10 meV. This is due to the difficulty of extracting, by profile fitting, correct energy-transfer values for the phonon peaks because of the modest intensity of the signal, which is a consequence of the small scattering cross section. The experimental branch is unambiguously characterized up to $\chi = 0.24$, and at energy transfers greater than 16 meV the observed signal is a mixture of acoustic and low-energy optic branches.

Figure 3b shows the transverse acoustic branch along the same direction as the curve in Figure 3a. It may be unambiguously assigned to a transverse mode, and the agreement between observed and calculated data is satisfactory, although the theoretical frequencies are slightly overestimated with respect to the experimental values. The disagreement is more evident for energies higher than 12 meV because the analysis of the observed signal becomes more complex owing to the partial superposition of the transverse and longitudinal modes, as demonstrated by the simulated data. The experimental points lie approximately on a straight line and allow an obvious choice between the two calculated modes.

Figure 3c shows the acoustic transverse mode along the reciprocal lattice direction [001], indexed according to the primitive cell. The calculated acoustic transverse modes are nearly degenerate, and the resolution of the instrument does not permit their differentiation. Nevertheless, the simulation allows us to recognize the observed branch unequivocally, as explained in the next paragraph. Agreement between theoretical and experimental data is, on the whole, quite satisfactory given that the employed potential was not optimized for the observed modes. Moreover, the complexity of the system, the multiphonon effect, the weakness of the scattering intensity for each anelastic process, and the impurities (which limit the resolution) all make data analysis rather difficult.

From the classical theory of elasticity, the elastic constants are related simply to the phonon wave-vector components by the following expression (Dove 1993; Wallace 1972):

$$|\rho\omega^2\delta_{ij} - C_{ijlm}\mathbf{q}_m\mathbf{q}_l| = |T_{ij}| = 0 \qquad (3)$$

Table 1. Observed and calculated vibrational frequencies of acoustic transverse (TA) and longitudinal (LA) modes at the $\chi[ijk]$ point of reciprocal space

LA[$\bar{1}$11]			TA[$\bar{1}$11]			TA[001]		
χ	Obs.	Calc.	χ	Obs.	Calc.	χ	Obs.	Calc.
0.042	4.2	3.1	0.051	2.8	2.0	0.063	2.4	1.8
0.053	5.1	3.8	0.101	5.4	3.8	0.076	1.8	2.2
0.054	4.4	3.9	0.138	6.6	5.2	0.089	2.5	2.6
0.075	5.9	5.5	0.176	7.8	6.5	0.094	3.0	2.7
0.095	6.8	6.9	0.196	8.4	7.2	0.102	3.1	3.0
0.095	6.9	6.9	0.223	9.2	8.0	0.114	3.6	3.3
0.106	7.8	7.6	0.227	8.9	8.2	0.118	2.5	3.4
0.109	9.4	7.8	0.273	11.0	9.6	0.131	4.2	3.8
0.112	8.8	8.0	0.303	11.9	10.4	0.142	4.6	4.1
0.126	9.8	8.9	0.339	12.8	11.4	0.148	3.3	4.3
0.128	10.3	9.1	0.376	13.7	12.3	0.193	5.6	5.5
0.136	8.6	9.6	0.407	14.7	13.0	0.235	6.3	6.6
0.149	11.2	10.4	0.448	15.6	13.6	0.240	6.9	6.7
0.156	9.8	10.8	0.494	16.5	13.5	0.271	7.3	7.5
0.160	12.2	11.1				0.308	8.2	8.4
0.179	13.2	12.1				0.318	8.8	8.6
0.191	14.2	12.6				0.354	9.1	9.4
0.198	12.2	12.9				0.355	9.4	9.4
0.231	15.0	13.6				0.380	9.2	9.9
						0.431	10.3	10.8
						0.484	11.3	11.4

Note: Directions and units refer to the reciprocal primitive cell; χ refers to the fractional coordinates of the **q** vector along the corresponding symmetry direction. Frequencies are in millielectron volts.

where vertical bars indicate the determinant of the matrix T_{ij}, ρ is the density of the compound, ω is the acoustic vibrational frequency, and **q** has the same meaning as above. The elastic constants are indexed according to a full tensorial formalism, although hereafter the contracted Voigt formalism (see, for example, Born and Huang 1954) is used for the sake of simplicity. The summation is performed on repeated indexes according to the usual convention. Generally, the relation between the **q** components and the elastic constants is quite complex, but it is simplified in the case of cubic symmetry and for particular reciprocal space directions. It is obvious that, for cubic symmetry, the slopes of the acoustic branches, evaluated at the zone center, are directly related to the elastic constants or to linear combinations of them. For **q** along the $[\bar{1}11]$ direction (indexed according to the primitive cell) we have

$$C_{ij} = \rho\left(\frac{d\omega}{d|\mathbf{q}|}\right)^2 \qquad (4)$$

where the calculation is performed with respect to longitudinal or transverse branches to evaluate C_{11} or C_{44}, respectively. When **q** lies along the [001] direction (with respect to the primitive cell), the slopes of the three nondegenerate acoustic branches allow us to estimate C_{44} and $\frac{1}{2}(C_{11} - C_{12})$, by transverse modes, and $\frac{1}{2}(C_{11} + C_{12} + 2C_{44})$, by the longitudinal mode, following a procedure analogous to that shown above. A straight line was fitted to each measured branch, and the elastic constants, or a linear combination of them, are extracted by the angular coefficient. Table 2 reports the results of such an analysis together with the most recent experimental data for py-

TABLE 2. Experimental and calculated elastic constants

	Present work	Calc.	Data set A
C_{11}	340(20)	329	296.2(5)
C_{44}	95(5)	96	91.6(3)
$C_{11} - C_{12}$	186(8)	195	185.1(8)

Note: Elastic constants estimated by the slope of acoustic branches at the zone center (present work), as calculated by the potential discussed in the text, and as measured through Brillouin scattering (A) (O'Neill et al. 1991). Units in gigapascals.

rope (O'Neill et al. 1991), hereafter indicated as data set A, and with the values of the elastic constants derived from our theoretical calculations. The elastic constant C_{11}, evaluated by neutrons, deviates about 15% from the corresponding value in data set A, whereas good agreement exists with the simulated data. The low intensity of the longitudinal phonon signal, and consequently the error in the estimated energy values, may be the reason for the disagreement, since we have more confidence in the published experimental values of the elastic constants. The calculated values deviate slightly from those reported by Winkler et al. (1991) because we used the structural parameters for pyrope derived from the single-crystal neutron diffraction analysis on the Dora Maira sample.

Agreement among the three data sets reported in Table 2 for the C_{44} elastic constant is quite satisfactory, and our result deviates from the one in set A by <4%. In this case the excellent quality of the observed phonon signals allows us to define the branch well, reducing the positional error of the experimental points in the **Q**-ω plane. Also, in the case of the linear combination $C_{11} - C_{12}$, the value measured by the slope of the acoustic phonon branch matches the observed value in data set A very well, and a reasonable agreement exists with the result of the simulation. In this case, we analyzed the slope of the branch measured along the [001] direction. Two, nearly degenerate, acoustic transverse modes and one longitudinal mode are present. A previous inspection of eigenvectors allowed us to distinguish between longitudinal and transverse modes. With the direction of vibration of each transverse mode from theoretical calculations and the corresponding relation with the elastic constants, we assigned the observed branch to the transverse acoustic mode, on the basis of the calculated inelastic cross section, yielding information on the $C_{11} - C_{12}$ linear combination.

On the whole, taking into account (1) that the low neutron cross section required the use of a large crystal obviously containing a large density of defects, (2) the many modes per each point of the Brillouin zone (240 in our system), and (3) the lower resolution of the PRISMA spectrometer with respect to a triple-axis instrument, the present results may be considered a success and constitute the basis for further investigations. Furthermore, the present data are the first of their kind for such a complicated system.

ACKNOWLEDGMENTS

Financial support was provided by Italian MURST and CNR. The authors wish to thank U. Steigenberger for assistance in the measurements, and M. Dove, S. Ghose, and N. Ross for useful comments that improved the manuscript. Provision of neutron scattering facilities by the Daresbury and Rutherford Appleton Laboratories (DRAL) is gratefully acknowledged.

REFERENCES CITED

Andreani, C., Carlile, C.J., Cilloco, F., Petrillo, C., Sacchetti, F., Stirling, G.C., and Windsor, C.G. (1987) PRISMA: A spectrometer for the measurement of coherent excitations on a pulsed spallation neutron source. Nuclear and Instrumentation Methods, A254, 333–341.

Armbruster, T., Geiger, C.A., and Lager, G.A. (1992) Single-crystal X-ray structure study of synthetic pyrope almandine garnets at 100 and 293 K. American Mineralogist, 77, 512–521.

Bialas, H., and Stolz, H.J. (1975) Lattice dynamics of sapphire (corundum). Zeitschrift für Physik, B21, 319–324.

Born, M., and Huang, J. (1954) The dynamical theory of crystal lattices, 420 p. Clarendon, Oxford, U.K.

Böttger, H. (1983) Principles of the theory of lattice dynamics, 330 p. Physik-Verlag, Weinheim, Germany.

Boysen, H. (1980) Dynamic structure determination for two interacting modes at the M-point in α- and β-quartz by inelastic neutron scattering. Journal of Physics, C13, 6127–6146.

——(1990) Neutron scattering and phase transition in leucite. In E.K.H. Salje, Ed., Phase transition in ferroelastic and co-elastic crystals, 334 p. Cambridge University Press, Cambridge.

Boysen, H., Frey, F., Schrader, H., and Eckold, G. (1991) On the proto- to ortho-/clino enstatite phase transformation: Single crystal X-ray and inelastic neutron investigation. Physics and Chemistry of Minerals, 17, 629–635.

Catlow, C.R.A. (1988) Computer modelling of silicates. In NATO ASI series C, 225, 619–638.

Catlow, C.R.A., James, R., Mackrodt, J.R., and Stewart, R.F. (1982) Defect energies in aluminum oxide and rutile titanium oxide. Physical Review B, 25, 1006–1026.

Catti, M., Pavese, A., and Price, G.D. (1993) Thermodynamic properties of $CaCO_3$ calcite and aragonite: A quasi-harmonic calculation. Physics and Chemistry of Minerals, 20, 472–479.

Chopin, C. (1984) Coesite and pure pyrope in high-grade blueschists of the Western Alps: A first record and some consequences. Contributions to Mineralogy and Petrology, 86, 107–118.

Collins, D.R., Stirling, W.G., Catlow, C.R.A., and Rowbotham, G. (1993) Determination of acoustic phonon dispersion curves in layer silicates by inelastic neutron scattering and computer simulation techniques. Physics and Chemistry of Minerals, 19, 520–527.

Cowley, E.R., and Pant, A.K. (1973) Lattice dynamics of calcite. Physical Review B, 8, 4795–4800.

Dove, M.T. (1993) Introduction to lattice dynamics, 258 p. Cambridge University Press, Cambridge.

Dove, M.T., Hagen, M., Harris, M.J., Powell, B.M., Steigenberger, U., and Winkler, B. (1992) Anomalous inelastic neutron scattering from calcite. Journal of Physics of Condensed Matter, 4, 2761–2774.

Elcombe, M.M. (1967) Some aspects of the lattice dynamics of quartz. Proceedings of the Physical Society of London, 91, 947–958.

Ghose, S., Hastings, J.M., Corliss, L.M., Rao, K.R., Chaplot S.L., and Choudury, N. (1987) Study of the phonon dispersion relations in forsterite, Mg_2SiO_4, by inelastic neutron scattering. Solid State Communications, 63, 1045–1050.

Ghose, S., Hastings, J.M., Choudhury, N., Chaplot, S.L., and Rao, K.R. (1991) Phonon dispersion relation in fayalite, Fe_2SiO_4. Physica B, 174, 83–86.

Ghose, S., Choudhury, N., Chaplot, S.L., and Rao, K.R. (1992) The phonon density of states and thermodynamic properties of minerals. In Advances in Physical Geochemistry, 10, 283–314.

Hagen, M. (1994) PRSCAL manual. Rutherford Appleton Laboratory Report RAL-94-084.

Hagen, M., Dove, M.T., Harris, M.J., Steigenberger, U., and Powell, B.P. (1992) Orientational order-disorder phase transition in calcite. Physica B, 180, 276–278.

Haselton, H.T., and Westrum, E.F. (1980) Low temperature heat capacities of synthetic pyrope, grossular, and pyrope$_{60}$grossular$_{40}$. Geochimica et Cosmochimica Acta, 44, 701–709.

Hofmeister, A.M., and Chopelas, A. (1991) Thermodynamic properties of pyrope and grossular from vibrational spectroscopy. American Mineralogist, 76, 880–891.

Line, C.M.B., Winkler, B., and Dove, M.T. (1994) Quasielastic incoherent neutron scattering study of the rotational dynamics of the water molecules in analcime. Physics and Chemistry of Minerals, 21, 451–459.

Lovesey, S.W. (1984) Theory of neutron scattering from condensed matter, p. 98–169. Clarendon, Oxford, U.K.

O'Neill, B., Bass, J.D., Rossman, G.R., Geiger, C.A., and Langer, K. (1991) Elastic properties of pyrope. Physics and Chemistry of Minerals, 17, 617–621.

Parker, S.C., and Price, G.D. (1988) Computer modelling of phase transitions in minerals. Advances in Solid-State Chemistry, 1, 295–327.

Pavese, A., Catti, M., Price, G.D., and Jackson, R.A. (1992) Interatomic potentials for $CaCO_3$ polymorphs (calcite and aragonite), fitted to elastic and vibrational data. Physics and Chemistry of Minerals, 19, 80–87.

Pavese, A., Artioli, G., and Prencipe, M. (1995) X-ray single-crystal diffraction study of pyrope in the temperature range 30–973 K. American Mineralogist, 80, 457–464.

Pilati, T., Demartin, F., and Gramaccioli, C.M. (1993a) Atomic thermal parameters and thermodynamic functions for corundum (a-Al_2O_3) and bromellite (BeO): A lattice-dynamical estimate. Acta Crystallographica, A49, 473–480.

Pilati, T., Demartin, F., Criati, F., Bruni, S., and Gramaccioli, C.M. (1993b) Atomic thermal parameters and thermodynamic functions for crysoberyl ($BeAl_2O_4$) from vibrational spectra and transfer of empirical force fields. Acta Crystallographica, B49, 216–222.

Price, D.L., Ghose, S., Choudhury, N., Chaplot, S.L., and Rao, K.R. (1991) Phonon density of states in fayalite, Fe_2SiO_4. Physica B, 174, 87–90.

Rao, K.R., Chaplot, S.L., Choudury, N., Ghose, S., Hastings, J.M., and Corliss, L.M. (1988) Lattice dynamics and inelastic neutron scattering from forsterite, Mg_2SiO_4: Phonon dispersion relation, density of states and specific heat. Physics and Chemistry of Minerals, 16, 83–97.

Sacchetti, F., Petrillo, C., and Moze, O. (1994) Temperature dependence of phonon intensities in tantalum below 4.2 K. Physical Review B, 49, 8747–8750.

Salje, E., and Werneke, C. (1982) How to determine phase stabilities from lattice vibrations. In W. Schreyer, Ed., High-pressure researches in geosciences, p. 321–348. Scheweitzerbart'sche Verlagsbuch-handlung, Stuttgart, Germany.

Sanders, M.J., Leslie, M., and Catlow, C.R.A. (1984) Interatomic potential for SiO_2. Journal of the Chemical Society, Chemical Communications, 1271–1273.

Schertl, H.P., Schreyer, W., and Chopin, C. (1991) The pyrope-coesite rocks and their country rocks at Parigi, Dora Maira massif, Western Alps: Detailed petrography, mineral chemistry, and metamorphic evolution. Contributions to Mineralogy and Petrology, 108, 1–21.

Schober, H., Strauch, D., and Dorner, B. (1993) Lattice dynamics of sapphire (Al_2O_3). Zeitschrift für Physik, B92, 273–283.

Steigenberger, U., Hagen, M., Caciuffo, R., Petrillo, C., Cilloco, F., and Sacchetti, F. (1991) The development of the PRISMA spectrometer at ISIS. Nuclear and Instrumentation Methods, B53, 87–96.

Strauch, D., and Dorner, B. (1993) Lattice dynamics of a-quartz: I. Experiment. Journal of Physics of Condensed Matter, 5, 6149–6154.

Wall, A., Parker, S.C., and Watson, G.W. (1993) The extrapolation of elastic moduli to high pressure and temperature. Physics and Chemistry of Minerals, 20, 69–75.

Wallace, D.C. (1972) Thermodynamics of crystals, 440 p. Wiley, New York.

Winkler, B., and Buehrer, W. (1990) Lattice dynamics of andalusite: Prediction and experiment. Physics and Chemistry of Minerals, 17, 453–461.

Winkler, B., Dove, M.T., and Leslie, M. (1991) Static lattice energy minimization and lattice dynamics calculations on aluminosilicate minerals. American Mineralogist, 76, 313–331.

Manuscript received March 7, 1995
Manuscript accepted September 14, 1995